

Stability of an electromagnetically levitated spherical sample in a set of coaxial circular loops

Jānis Priede and Gunter Gerbeth

Abstract—This paper presents a theoretical study of oscillatory and rotational instabilities of a solid spherical body levitated electromagnetically in axisymmetric coils made of coaxial circular loops. We apply our previous theory to analyze the static and dynamic stability of the sample depending on the AC frequency and the position of the sample in the coils for several simple configurations. An original analytical approach is introduced employing a gauge transformation for the vector potential. First we calculate the spring constants which define the frequency of small-amplitude oscillations. For static stability the spring constants must be positive. Dynamic instabilities are characterized by critical AC frequencies which, when exceeded, may result either in a spin-up or oscillations with increasing amplitude. It is found that the critical frequencies increase with the non-uniformity of the field. We show that for a spherically harmonic field the critical frequency for the spin-up instability in a field of degree l coincides with the critical frequency for the oscillatory instability in a field of degree $l + 1$.

I. INTRODUCTION

ELECTROMAGNETIC levitation melting (ELM) was invented in the twenties of the last century [1] whereas its usage started only at the beginning of the fifties [2] when high-frequency power generators became available. The basic principle of ELM is simple: a conducting sample, usually metallic, weighting from several tens of grams up to several kilograms is placed in a coil fed by an AC current with a typical frequency ranging from about 10 kHz up to several 100 kHz . The AC magnetic field induces eddy currents in the sample which, in turn, give rise to two effects. On one hand, eddy currents interact with those in the coil giving rise to a Lorentz force that repels the sample from the coil. On the other hand, the Ohmic dissipation due to the induced currents provides heating of the sample. In such a way, the sample can be levitated and also melted, provided that the coil configuration and the current in it are properly adjusted. ELM is particularly useful for melting reactive metals with high melting points, for example such as Ti , Zr , V , Ta , Mo , which often react with the crucible material and so get polluted by it [2]. ELM avoids contamination of the melt and allows one to carry out solidification from deeply under-cooled states

which is of interest for certain material science applications [3]. Besides, ELM is a well-known method for measurements of material properties of liquid metals used on ground as well as in space [4], [5].

The balance of gravity and electromagnetic forces is necessary but not sufficient for a successful levitation. In addition, the sample has to be stable at least to perturbations of sufficiently small amplitude. First, it means that the reaction force due to the displacement of the sample from its equilibrium position has to act against that displacement. Otherwise, the equilibrium will be statically unstable and the solid sample will fall out of the coil or touch it when it is slightly perturbed. Similarly, a molten sample may leak out of the coil in the result of surface folding and deformation [6]. The static stability alone may also be insufficient for a successful levitation because sometimes the sample exhibits overstability. Namely, there is a restoring force that makes the sample to execute oscillations with increasing amplitude so that the sample eventually hits the coil or leaves it [2]. Similarly, sometimes the sample is observed to spin-up [2], [7], [8]. A purely electromagnetic theory trying to account for such dynamic instabilities has been proposed in our previous work and applied to some simple configurations of magnetic fields [9], [10]. In this study, we apply our previous theory to analyze both the static and dynamic stability of a spherical sample in more realistic axisymmetric magnetic systems made of a set of coaxial circular current loops. Although the basic configuration is axisymmetric, the perturbation fields are, in general, three-dimensional that renders the problem mathematically more complicated. To calculate 3D fields for a spherical sample we use similar analytic techniques as in Refs. [11], [12]. However, our approach differs from the previous ones by an original use of the gauge transformation for the 3D vector potential in order to satisfy boundary conditions for the induced current. This allows us to carry out the analysis only in terms of the vector potential without considering the scalar electrostatic potential. Therefore our approach is considerably simpler compared to [11], [12].

The paper is organized as follows. The stability of small amplitude oscillations of arbitrary direction is considered in Sec. 2 beginning with the governing equations and analytic solutions for the vector potential of a circular current loop in spherical harmonics. In this section we also derive solutions for the axisymmetric base state and the perturbation field due to a small displacement. Section 3 presents governing equations and analytic solution for the spin-up instability. Numerical results for both instabilities in several simple inductors

Manuscript received December 13, 2004; revised February 24, 2005. This work was supported by Deutsche Forschungsgemeinschaft in frame of the Collaborative Research Centre SFB 609 and by the European Commission under grant No. G1MA-CT-2002-04046.

J. Priede was with Forschungszentrum Rossendorf, P.O. Box 510119, 01314 Dresden, Germany during this work. Presently he is with the Institute of Physics, University of Latvia, Miera st. 32, LV-2169 Salaspils, Latvia;

G. Gerbeth is with Forschungszentrum Rossendorf, MHD Department, P.O. Box 510119, 01314 Dresden, Germany

are discussed in Section 4 and summarized in Section 5.

II. SMALL-AMPLITUDE OSCILLATIONS

A. Formulation of the problem and governing equations

Consider a sphere with radius R and conductivity σ moving at velocity \mathbf{v} in a magnetic field \mathbf{B} alternating with circular frequency ω . The induced electric field follows from the first Maxwell equation as $\mathbf{E} = -\nabla\Phi - \partial_t\mathbf{A}$, where Φ is the scalar potential of the electric field and \mathbf{A} is the vector potential of the magnetic field. The density of the electric current induced in a moving medium is given by Ohm's law

$$\mathbf{j} = \sigma(\mathbf{E} + \mathbf{v} \times \mathbf{B}) = \sigma(-\nabla\Phi - \partial_t\mathbf{A} + \mathbf{v} \times \nabla \times \mathbf{A}).$$

The electric field induced by a translational solid body motion with \mathbf{v} being a spatially invariant vector can be represented as

$$\mathbf{v} \times \nabla \times \mathbf{A} = \nabla(\mathbf{v} \cdot \mathbf{A}) - (\mathbf{v} \cdot \nabla)\mathbf{A}.$$

Assuming that the frequency of the alternating magnetic field is sufficiently low to neglect the displacement current, the second Maxwell equation leads to the following advection-diffusion equation

$$\partial_t\mathbf{A} + (\mathbf{v} \cdot \nabla)\mathbf{A} = \frac{1}{\mu_0\sigma}\nabla^2\mathbf{A} \quad (1)$$

where the gauge invariance of \mathbf{A} has been employed to define the scalar potential as

$$\Phi = \mathbf{v} \cdot \mathbf{A} - \frac{1}{\mu_0\sigma}\nabla \cdot \mathbf{A}. \quad (2)$$

Boundary conditions at the surface follow from the continuity of the magnetic field

$$[\mathbf{A}_0]_S = [\partial_n\mathbf{A}_0]_S = 0 \quad (3)$$

where $[f]_S$ denotes a jump of the quantity f across the boundary S ; $\partial_n \equiv (\mathbf{n} \cdot \nabla)$ is the derivate normal to the boundary.

B. Analytical solution

1) Magnetic field of a circular loop in spherical harmonics:

The magnetic field of an inductor consisting of a set of coaxial circular loops represents a superposition of the fields of the separate loops. Therefore, we first consider a single loop lying parallel to the $x-y$ plane and centered with respect to the z -axis of a Cartesian coordinate system with a sphere at its origin, see Fig. 1. Approximation of a toroidal inductor of small cross-section by a circular loop is considered in more detail in Appendix 1. The loop is supplied with an AC current with amplitude I_0 alternating harmonically with a circular frequency ω as $I_0 \cos(\omega t)$. Henceforth we use the magnetic diffusion time $\tau_m = \mu_0\sigma R^2$ and the radius of the sphere R as time and length scales while the current density and the vector potential are scaled by I_0/R^2 and $\mu_0 I_0$, respectively. In the following, we assume all quantities to be dimensionless with the same notation as for the dimensional counterparts used so far. Further we consider the vector potential generated by the loop $\mathbf{A}^e(\mathbf{r}, t) = \mathbf{A}_0^e(\mathbf{r}) \cos(\bar{\omega} t)$ with the axisymmetric amplitude $\mathbf{A}_0^e(\mathbf{r})$, where $\bar{\omega} = \omega\mu_0\sigma R^2$ is the dimensionless

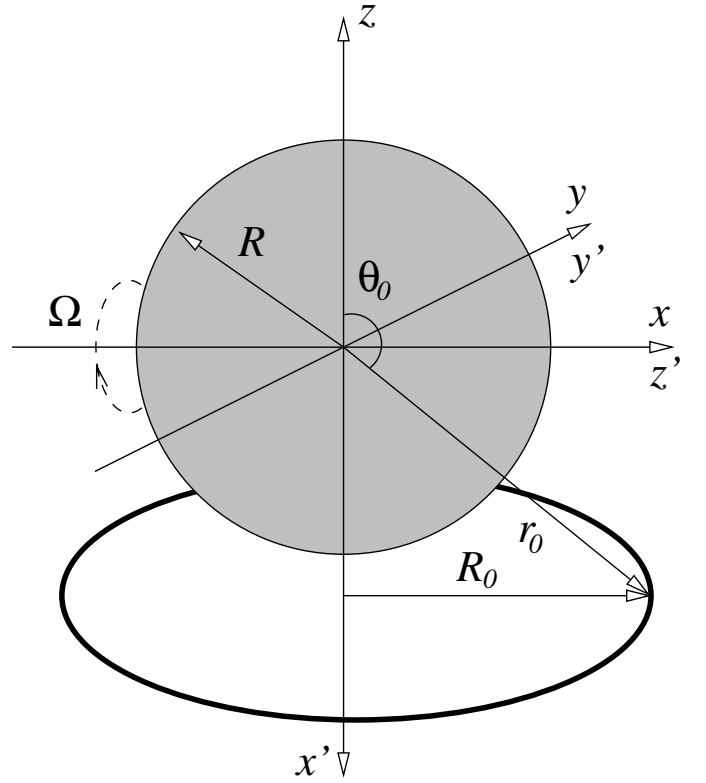


Fig. 1. Sketch to the formulation of the problem.

AC frequency which will be the main parameter throughout this paper.

The amplitude of the current density of such a loop can be represented by using the Dirac δ function:

$$\mathbf{j}_0^e(\mathbf{r}) = \mathbf{e}_\phi \delta(\theta - \theta_0) \delta(r - r_0) / r_0$$

where θ_0 and r_0 are the meridional angle and the spherical radius of the loop with respect to the center of the sphere as shown in Fig. 1. Further, it is advantageous to introduce a complex unit vector $\mathbf{e}_\eta = \frac{1}{\sqrt{2}}(\mathbf{e}_x + i\mathbf{e}_y)$ that allows us to represent the azimuthal unit vector as

$$\mathbf{e}_\phi = \frac{i}{\sqrt{2}}(\mathbf{e}_\eta^* e^{i\phi} - \mathbf{e}_\eta e^{-i\phi}),$$

where \mathbf{e}_x and \mathbf{e}_y are x and y unit vectors, respectively, and the asterisk denotes the complex conjugate. Then the current density can be expanded in spherical harmonics as

$$\begin{aligned} \mathbf{j}_0^e(\mathbf{r}) = & -\sqrt{2}\pi \sin\theta_0 \delta(r - r_0) / r_0 \\ & \times \sum_{l=1}^{\infty} Y_{l1}(\theta_0, 0) \sum_{m=-1}^1 \mathbf{I}^m Y_{lm}(\theta, \phi), \end{aligned} \quad (4)$$

where $Y_{lm}(\theta, \phi)$ are spherical harmonics as defined in [14]. The expansion coefficients are

$$\mathbf{I}^m = \begin{cases} 0; & m \neq \pm 1 \\ i\mathbf{e}_\eta^*; & m = 1 \\ i\mathbf{e}_\eta; & m = -1 \end{cases}.$$

Using the generating function of the spherical harmonics [14] the vector potential of a circular loop is obtained as

$$\mathbf{A}_0^e(\mathbf{r}) = \sqrt{2\pi}R_0 \sum_{l=1}^{\infty} \frac{Y_{l1}(\theta_0, 0)}{2l+1} \frac{(r, r_0)_{<}^l}{(r, r_0)_{>}^{l+1}} \times \sum_{m=-1}^1 \mathbf{I}^m Y_{lm}(\theta, \phi), \quad (5)$$

where $R_0 = r_0 \sin \theta_0$ is the cylindrical radius of the loop; $(r, r')_{<} = \min(|\mathbf{r}|, |\mathbf{r}'|)$; $(r, r')_{>} = \max(|\mathbf{r}|, |\mathbf{r}'|)$. In order to facilitate the following algebra, it is advantageous to introduce the functions $X_l^m(\mathbf{r}) = r^{-l-1} Y_{lm}(\theta, \phi)$ and $\bar{X}_l^m(\mathbf{r}) = r^l Y_{lm}(\theta, \phi)$, which are the outer and the inner solutions of the Laplace equation associated to the spherical harmonic $Y_{lm}(\theta, \phi)$. Basic properties of those functions are given in Appendix 2. For the region occupied by the sphere ($r < r_0$) the solution above takes the form

$$\mathbf{A}_0^e(\mathbf{r}) = \sqrt{2\pi}R_0 \sum_{l=1}^{\infty} \frac{X_l^1(\mathbf{r}_0)}{2l+1} \sum_{m=-1}^1 \mathbf{I}^m \bar{X}_l^m(\mathbf{r})$$

where $\phi_0 = 0$ for \mathbf{r}_0 is assumed.

2) *Axisymmetric basic state:* For a sphere at rest the vector potential is sought as $\mathbf{A}(\mathbf{r}, t) = \Re[\mathbf{A}_0(\mathbf{r})e^{i\omega t}]$, where \mathbf{A}_0 is complex. For the interior of the sphere, (1) takes the form

$$\nabla^2 \mathbf{A}_0 = i\bar{\omega} \mathbf{A}_0 \quad (6)$$

while for the exterior we have

$$\nabla^2 \mathbf{A}_0 = 0 \quad (7)$$

whereas (2) takes the form of the Coulomb gauge $\nabla \cdot \mathbf{A}_0 = 0$. For the interior, the solution is

$$\mathbf{A}_0(\mathbf{r}) = \sqrt{2\pi}R_0 \sum_{l=1}^{\infty} \frac{X_l^1(\mathbf{r}_0)}{2l+1} \bar{g}_l j_l(r\sqrt{\bar{\omega}/i}) \times \sum_{m=-1}^1 \mathbf{I}^m Y_{lm}(\theta, \phi) \quad (8)$$

where \bar{g}_l are unknown coefficients to be determined from the boundary conditions; $j_l(x)$ is the spherical Bessel function of index l [13]. For the exterior, the solution is represented as a superposition of external and induced fields $\mathbf{A}_0(\mathbf{r}) = \mathbf{A}_0^e(\mathbf{r}) + \mathbf{A}_0^i(\mathbf{r})$ where the latter is sought as

$$\mathbf{A}_0^i(\mathbf{r}) = \sqrt{2\pi}R_0 \sum_{l=1}^{\infty} \frac{X_l^1(\mathbf{r}_0)}{2l+1} g_l \sum_{m=-1}^1 \mathbf{I}^m X_l^m(\mathbf{r}). \quad (9)$$

From the conditions (3) applied at the surface of the sphere at $r = 1$ we find

$$\bar{g}_l = \frac{2l+1}{\sqrt{\bar{\omega}/i}} \frac{1}{j_{l-1}(\sqrt{\bar{\omega}/i})}; \quad g_l = \frac{j_{l+1}(\sqrt{\bar{\omega}/i})}{j_{l-1}(\sqrt{\bar{\omega}/i})}.$$

Some useful properties and an efficient algorithm for the calculation of $g_l(x)$ and its derivative are given in Appendix 3.

The time-averaged total force on the sphere is

$$\mathbf{F}_0 = \int_V \langle \mathbf{j} \times \mathbf{B} \rangle dV = \frac{1}{2} \int_V \Re[\mathbf{j}_0 \times \mathbf{B}_0^*] dV,$$

where the integral is taken over the volume of the sphere V . Taking into account that $\mathbf{j}_0 = \nabla \times \mathbf{B}_0^i$ and $\mathbf{B}_0 = \mathbf{B}_0^e + \mathbf{B}_0^i$, where \mathbf{B}_0^e is a purely real quantity, we obtain $\mathbf{F}_0 = \frac{1}{2} \int_V \Re[\mathbf{j}_0] \times \mathbf{B}_0^e dV$. According to the momentum conservation law the force exerted by a magnetic field on a body is opposite to that exerted by the body on the source of the magnetic field $\mathbf{F}_0 = -\frac{1}{2} \int_V \mathbf{j}_0^e \times \Re[\mathbf{B}_0^i] dV$ where the integral is taken over the space outside the sphere \bar{V} . The last integral can be taken straightforwardly because the external current (4) is defined in terms of a Dirac δ function. Taking into account that the induced magnetic field outside the sphere is

$$\mathbf{B}_0^i = \sqrt{2\pi}R_0 \sum_{l=2}^{\infty} \frac{X_{l-1}^1(\mathbf{r}_0)}{2l-1} g_{l-1} \sum_{m=-2}^2 N_l^m X_l^m \times \left(\frac{\mathbf{e}_\eta^* \times \mathbf{I}^{m-1}}{\sqrt{2}N_{l-1}^{m-1}} - \frac{\mathbf{e}_\eta \times \mathbf{I}^{m+1}}{\sqrt{2}N_{l-1}^{m+1}} - \frac{\mathbf{e}_z \times \mathbf{I}^m}{N_{l-1}^m} \right)$$

where $N_l^m = \sqrt{\frac{(l-m)!(l+m)!}{2l+1}}$, we find

$$\mathbf{F}_0 = \mathbf{e}_z \pi \sum_{l=2}^{\infty} \Re[g_{l-1}] f_{l-1} f_l \left(\frac{l^2-1}{4l^2-1} \right)^{1/2} \quad (10)$$

where $f_l = r_0^{-l} \sin \theta_0 \bar{P}_l^1(\cos \theta_0)$ involves the normalised Legendre function $\bar{P}_l^m(x)$ related to the spherical harmonics as $Y_{lm}(\theta, \phi) = \frac{(-1)^m}{\sqrt{2\pi}} \bar{P}_l^m(\cos \theta) e^{im\phi}$ [13]. In case of N current loops we have

$$f_l = \sum_{n=1}^N I_n r_n^{-l} \sin \theta_n \bar{P}_l^1(\cos \theta_n) \quad (11)$$

where I_n is the dimensionless current carried by the n -th loop; R_n , r_n , and θ_n are defined analogously as for the single loop. Note that the solution (10) alone could be obtained in a simpler way as in Ref. [15]. Our following analysis, however, is aimed at non-axisymmetric solutions which require a more complicated algebra.

3) *Perturbation due to a small displacement:* Consider a small displacement \mathbf{x} of the center of the sphere from the position \mathbf{r} to $\mathbf{r} + \mathbf{x}$. In the frame of reference related to the sphere, this corresponds to a perturbation of the external magnetic field

$$\mathbf{A}_0^e(\mathbf{r} + \mathbf{x}) \approx \mathbf{A}_0^e(\mathbf{r}) + (\mathbf{x} \cdot \nabla) \mathbf{A}_0^e(\mathbf{r}) = \mathbf{A}_0^e(\mathbf{r}) + |\mathbf{x}| \mathbf{A}_1^e(\mathbf{r}),$$

where

$$\mathbf{A}_1^e(\mathbf{r}) = (\boldsymbol{\epsilon}_x \cdot \nabla) \mathbf{A}_0^e(\mathbf{r}) = \sqrt{2\pi}R_0 \sum_{l=0}^{\infty} \frac{X_{l+1}^1(\mathbf{r}_0)}{2l+1} \sum_{m=-2}^2 \mathbf{J}_l^m \bar{X}_l^m(\mathbf{r})$$

$\boldsymbol{\epsilon}_x = \mathbf{x}/|\mathbf{x}|$ and

$$\mathbf{J}_l^m = \left(\mathbf{I}^{m-1} N_{l+1}^{m-1} \frac{(\boldsymbol{\epsilon}_x \cdot \mathbf{e}_\eta^*)}{\sqrt{2}} + \mathbf{I}^m N_{l+1}^m (\boldsymbol{\epsilon}_x \cdot \mathbf{e}_z) - \mathbf{I}^{m+1} N_{l+1}^{m+1} \frac{(\boldsymbol{\epsilon}_x \cdot \mathbf{e}_\eta)}{\sqrt{2}} \right) / N_l^m.$$

Now the external field represents a superposition of the axisymmetric base field $\mathbf{A}_0^e(\mathbf{r})$ and a small but in general

non-axisymmetric perturbation $\mathbf{A}_1^e(\mathbf{r})$. The perturbation of the inner field \mathbf{A}_1 is governed by the same Eqs. (6, 7) as the base field with the difference that now the external field is given by $\mathbf{A}_1^e(\mathbf{r})$. Consequently, the perturbation of the inner field and the corresponding induced field outside the sphere can be obtained straightforwardly by replacing the coefficients \mathbf{I}^m by \mathbf{J}_l^m in the corresponding solutions (8, 9) for the base field. Although the solution of the perturbed field obtained in such a way satisfies (6, 7) and the boundary conditions, it turns out that the induced field outside does not satisfy the Coulomb gauge unless the problem is axisymmetric, *i.e.*, the offset is along the symmetry axis. Thus, although the Laplace equation is satisfied we formally have $\nabla \times \nabla \times \mathbf{A}_1^i = \nabla \nabla \cdot \mathbf{A}_1^i = \mathbf{j}_1^i \neq 0$ which implies that the current is leaking outside the sphere. In addition note that the continuity of the tangential components of induction following from the continuity of the vector potential and its normal derivative at the surface of the sphere ensures continuity of the radial, *i.e.* normal, component of the current because $\mathbf{r} \cdot \mathbf{j} = \mathbf{r} \cdot \nabla \times \mathbf{B} = \nabla \cdot (\mathbf{B} \times \mathbf{r})$. Thus, the vector potential satisfying the Laplace equation and the Coloumb gauge outside the sphere and being continuous at the surface ensures that the current is closed in the sphere. As shown above, the induced vector potential unambiguously follows from the imposed one. Thus, the induced vector potential can be modified only by changing the imposed one. This can be done by employing the gauge invariance which allows us to add to the external vector potential $\mathbf{A}_1^e(\mathbf{r})$ a gradient of some gauge potential defined as

$$\Lambda_1^e(\mathbf{r}) = \sqrt{2\pi}R_0 \sum_{l=1}^{\infty} \frac{X_l^1(\mathbf{r}_0)}{2l+1} \sum_{m=-1}^1 \lambda_l^m \bar{X}_l^m(\mathbf{r}).$$

In order to fulfill the Coulomb gauge for the external vector potential, $\Lambda_1^e(\mathbf{r})$ has to be a harmonic function which is reflected in the expression above. So, we obtain a set of free coefficients λ_l^m which can be chosen to satisfy the Coulomb gauge for the induced field. This gauge transformation results in the replacement of the original coefficients \mathbf{J}_l^m by

$$\mathcal{J}_l^m = \left(\mathbf{J}_l^m + \frac{\mathbf{e}_\eta^*}{\sqrt{2}} N_{l+1}^{m-1} \lambda_{l+1}^{m-1} - \frac{\mathbf{e}_\eta}{\sqrt{2}} N_{l+1}^{m+1} \lambda_{l+1}^{m+1} + \mathbf{e}_z N_{l+1}^m \lambda_{l+1}^m \right) / N_l^m.$$

Then, similarly to the base field, the perturbation of the induced field is obtained as

$$\mathbf{A}_1^i(\mathbf{r}) = \sqrt{2\pi}R_0 \sum_{l=0}^{\infty} \frac{X_{l-1}^1(\mathbf{r}_0)}{2l-1} g_{l-1} \sum_{m=-2}^2 \mathcal{J}_l^m \bar{X}_l^m(\mathbf{r}).$$

From the Coulomb gauge we find

$$\lambda_l^m = (\boldsymbol{\epsilon}_x \cdot \mathbf{I}^m) \frac{2l-1}{(2l+1)l}.$$

The corresponding induction is

$$\begin{aligned} \mathbf{B}_1^i(\mathbf{r}) = & \sqrt{2\pi}R_0 \sum_{l=2}^{\infty} \frac{X_{l-1}^1(\mathbf{r}_0)}{2l-1} g_{l-1} \sum_{m=-3}^3 N_l^m X_l^m(\mathbf{r}) \\ & \times \left[\frac{\mathbf{e}_\eta^* \times \mathcal{J}_{l-1}^{m-1}}{\sqrt{2}N_{l-1}^{m-1}} - \frac{\mathbf{e}_\eta \times \mathcal{J}_{l-1}^{m+1}}{\sqrt{2}N_{l-1}^{m+1}} + \frac{\mathbf{e}_z \times \mathcal{J}_{l-1}^m}{N_{l-1}^m} \right]. \end{aligned}$$

According to our previous theory [10], small-amplitude oscillations of the sphere with $\mathbf{x}(t) = \mathbf{x}_0 \cos(\Omega t)$ give rise to a perturbation of the force on the sphere

$$\mathbf{F}_1 = \Re [(-\mathbf{K} + i\Omega \mathbf{\Gamma}) \cdot \mathbf{x}_0 e^{i\Omega t}] = -\mathbf{K} \cdot \mathbf{x} + \mathbf{\Gamma} \cdot \frac{d\mathbf{x}}{dt}.$$

where \mathbf{K} and $-\mathbf{\Gamma}$ are the effective electromagnetic stiffness and damping tensors, respectively. Further we refer to the elements of \mathbf{K} and $\mathbf{\Gamma}$ as the spring constants and growth rates, respectively. Note that due to the axial symmetry both \mathbf{K} and $\mathbf{\Gamma}$ are purely diagonal matrices with zero azimuthal components. At first, the axial symmetry implies that a purely axial displacement gives rise to a similar reaction force. Second, if the displacement is purely radial the reaction force, on the one hand, has to change to the opposite together with the displacement because of linearity but, on the other hand, it has to rotate around the symmetry axis together with the latter. Thus, a purely radial displacement causes a purely radial reaction force and, therefore, both \mathbf{K} and $\mathbf{\Gamma}$ are purely diagonal. Both diagonal elements of \mathbf{K} have to be positive for the static stability whereas the corresponding growth rates have to be negative for dynamic stability. Note that the growth rates can become positive and, thus, destabilizing when the dimensionless AC frequency exceeds a certain threshold depending on the configuration of the field [10]. Both the spring constants and the growth rates can be calculated for the given direction of the displacement specified by $\boldsymbol{\epsilon}_x = \mathbf{x}/|\mathbf{x}|$ by using the corresponding base and perturbation fields [10]:

$$\begin{aligned} \mathbf{K} \cdot \boldsymbol{\epsilon}_x &= -\frac{1}{2} \int_V [\Re [\mathbf{j}_1] \times \mathbf{B}_0^e + \Re [\mathbf{j}_0] \times \mathbf{B}_1^e] dV \\ \mathbf{\Gamma} \cdot \boldsymbol{\epsilon}_x &= \frac{1}{2} \partial_{\bar{\omega}} \int_V \Im [\mathbf{j}_1] \times \mathbf{B}_0^e dV. \end{aligned}$$

Similarly to the integral force, it is advantageous to change the region of integration from the sphere to the current loop

$$\begin{aligned} \mathbf{K} \cdot \boldsymbol{\epsilon}_x &= \frac{1}{2} \int_V [\mathbf{j}_0^e \times \Re [\mathbf{B}_1^i] + \mathbf{j}_1^e \times \Re [\mathbf{B}_0^i]] dV, \\ \mathbf{\Gamma} \cdot \boldsymbol{\epsilon}_x &= -\frac{1}{2} \partial_{\bar{\omega}} \int_V \mathbf{j}_0^e \times \Im [\mathbf{B}_1^i] dV. \end{aligned}$$

After some algebra we find

$$\begin{aligned} \mathbf{\Gamma} \cdot \boldsymbol{\epsilon}_x = & \pi \sum_{l=2}^{\infty} \Im [\partial_{\bar{\omega}} g_{l-1}] \frac{f_l^2}{2l+1} (l^2 - 1) \\ & \times \left[\frac{1}{2} \mathbf{e}_z \times \boldsymbol{\epsilon}_x \times \mathbf{e}_z (1 - \frac{1}{l}) + \mathbf{e}_z (\boldsymbol{\epsilon}_x \cdot \mathbf{e}_z) \right]. \end{aligned} \quad (12)$$

Taking into account that

$$\frac{1}{2} \int_V \mathbf{j}_1^e \times \mathbf{B}_0^i dV = -\frac{1}{2} \int_V \mathbf{j}_0^e \times (\boldsymbol{\epsilon}_x \cdot \nabla) \mathbf{B}_0^i dV$$

because $\mathbf{j}_1^e(\mathbf{r}) = (\boldsymbol{\epsilon}_x \cdot \nabla) \mathbf{j}_0^e(\mathbf{r})$, where $\mathbf{j}_0^e(\mathbf{r})$ is defined via

Dirac δ functions we eventually obtain

$$\begin{aligned} \mathbf{K} \cdot \boldsymbol{\epsilon}_x = & -\pi \sum_{l=2}^{\infty} \Re [g_{l-1}] \left\{ \frac{f_l^2}{2l+1} (l^2 - 1) \right. \\ & \times \left[\frac{1}{2} \mathbf{e}_z \times \boldsymbol{\epsilon}_x \times \mathbf{e}_z (1 - \frac{1}{l}) + \mathbf{e}_z (\boldsymbol{\epsilon}_x \cdot \mathbf{e}_z) \right] \\ & - \frac{f_{l-1} f_{l+1}}{2l-1} \left(\frac{l(l+2)(l^2-1)}{(2l-1)(2l+3)} \right)^{1/2} \\ & \left. \times \left[\frac{1}{2} \mathbf{e}_z \times \boldsymbol{\epsilon}_x \times \mathbf{e}_z - \mathbf{e}_z (\boldsymbol{\epsilon}_x \cdot \mathbf{e}_z) \right] \right\}. \end{aligned}$$

Now, we can use this series to calculate both the stiffness and the damping coefficients for a given coil defined by the coefficients f_l according to (11).

III. SPIN-UP INSTABILITY

A. Governing equations

We consider a solid sphere, as in Section 2, rotating with angular velocity $\boldsymbol{\Omega}$ in an alternating magnetic field. The density of the induced current is given by Ohm's law for a moving medium

$$\mathbf{j} = \sigma(\mathbf{E} + \mathbf{v} \times \mathbf{B}) = \sigma(-\partial_t \mathbf{A} - \nabla \Phi + \mathbf{v} \times \nabla \times \mathbf{A})$$

where $\mathbf{v} = \boldsymbol{\Omega} \times \mathbf{r}$ is the velocity of a solid-body rotation. The electric field induced by such a rotation may be represented as $\mathbf{v} \times \nabla \times \mathbf{A} = \nabla(\mathbf{v} \cdot \mathbf{A}) - (\mathbf{v} \cdot \nabla) \mathbf{A} - \mathbf{A} \times \boldsymbol{\Omega}$. Then from the second Maxwell equation with neglected displacement current, that corresponds to the quasistationary approximation assumed throughout this study, we obtain

$$\partial_t \mathbf{A} + (\mathbf{v} \cdot \nabla) \mathbf{A} + \mathbf{A} \times \boldsymbol{\Omega} = \frac{1}{\mu_0 \sigma} \nabla^2 \mathbf{A}.$$

Note that this equation governs the vector potential in the laboratory frame of reference where the body rotates while the source of the magnetic field is at rest. Further we proceed to the frame of reference rotating together with the sphere. In a rotating frame of reference, where the sphere is at rest while the source of the magnetic field rotates with velocity $-\mathbf{v}$, the equation above takes the form as for a body at rest

$$\partial_t \mathbf{A}(\mathbf{r}', t) = \frac{1}{\mu_0 \sigma} \nabla^2 \mathbf{A}(\mathbf{r}', t),$$

where \mathbf{r}' is a radius vector, which is time-dependent in the rotating frame of reference with $\partial_t \mathbf{r}' = \boldsymbol{\Omega} \times \mathbf{r}'$. In a rotating frame of reference, the body rotation appears as an additional time-dependence of the external magnetic field modulating the time-dependence of the applied magnetic field.

The time-averaged total torque on the sphere is

$$\mathbf{M} = \frac{1}{2} \int_V \mathbf{r} \times \Re [\mathbf{j}_0] \times \mathbf{B}_0^e dV.$$

According to the conservation of the angular momentum the torque exerted by the magnetic field on a body is opposite to that exerted by the body on the source of the magnetic field

$$\mathbf{M} = -\frac{1}{2} \int_V \mathbf{r} \times \mathbf{j}_0^e \times \Re [\mathbf{B}_0^i] dV,$$

where the integral is taken over the volume \bar{V} outside the sphere. The last integral can be taken straightforwardly because $\mathbf{j}_0^e(\mathbf{r}')$ is defined via Dirac δ functions. Because $(\mathbf{r} \cdot \mathbf{j}_0^e) = 0$ the integral above may be represented as

$$\mathbf{M} = -\frac{1}{2} \int_{\bar{V}} \mathbf{j}_0^e \Re [\mathbf{r} \cdot \nabla \times \mathbf{A}_0^i] dV$$

B. Analytical solution

Further we consider a sphere rotating about an axis perpendicular to the symmetry axis of an axisymmetric external magnetic field of a circular loop. The coordinate system related to the loop with the z axis as symmetry axis is chosen so that the rotation takes place about the x -axis, as shown in Fig. 1. It is convenient to analyze this rotation in a coordinate system turned about the y -axis by 90 degrees so that the z' -axis of the transformed coordinate system coincides with the original x -axis which is the axis of rotation and, respectively, the x' -axis is directed opposite to the z axis of the original coordinate system. Then the basis vectors of both coordinate systems are related as $\mathbf{e}'_x = -\mathbf{e}_z$, $\mathbf{e}'_y = \mathbf{e}_y$, and $\mathbf{e}'_z = \mathbf{e}_x$. Respectively, the complex unity vector is $\mathbf{e}_\eta = \frac{1}{2}(\mathbf{e}'_\eta - \mathbf{e}'_\eta^*) + \frac{\mathbf{e}'_z}{\sqrt{2}}$, where $\mathbf{e}'_\eta = \frac{1}{\sqrt{2}}(\mathbf{e}'_x + i\mathbf{e}'_y)$. To represent the vector potential of a circular loop in the turned coordinate system we use the addition theorem for Legendre polynomials [13] written as

$$\bar{X}_l^0(\mathbf{r}) = \sqrt{\frac{4\pi}{2l+1}} \sum_{m=-l}^l Y_{lm}(\pi/2, 0) \bar{X}_l^m(\mathbf{r}')$$

together with the relation

$$\bar{X}_l^1(\mathbf{r}) = \frac{2l+1}{2l+3} \frac{N_l^1}{N_{l+1}^0} \sqrt{2} (\mathbf{e}_\eta \cdot \nabla) \bar{X}_{l+1}^0(\mathbf{r})$$

which yields

$$\begin{aligned} \mathbf{A}_0^e(\mathbf{r}') = & \sqrt{2\pi} R_0 \sum_{l=1}^{\infty} \frac{X_l^1(\mathbf{r}_0)}{2l+1} \frac{N_l^1}{N_{l+1}^0} \sqrt{\frac{4\pi}{2l+3}} \\ & \times \sum_{m=-l}^l \mathbf{I}_l^m \bar{X}_l^m(\mathbf{r}') \end{aligned}$$

where

$$\begin{aligned} \mathbf{I}_l^m = & \frac{1}{N_l^m} [(\mathbf{e}'_\eta - \mathbf{e}'_\eta^*) N_{l+1}^m Y_{l+1,m}(\pi/2, 0) \\ & + i \frac{\mathbf{e}'_z}{\sqrt{2}} (N_{l+1}^{m-1} Y_{l+1,m-1}(\pi/2, 0) \\ & - N_{l+1}^{m+1} Y_{l+1,m+1}(\pi/2, 0))] . \end{aligned}$$

Similarly, the current density of the loop can be rewritten as

$$\begin{aligned} \mathbf{j}_0^e(\mathbf{r}') = & -\sqrt{2\pi} \sin \theta_0 \frac{\delta(r-r_0)}{r_0} \\ & \times \sum_{l=1}^{\infty} Y_{l1}(\theta_0, 0) \frac{N_l^1}{N_{l+1}^0} \sqrt{\frac{4\pi}{2l+3}} \\ & \times \sum_{m=-l}^l \mathbf{I}_l^m Y_{lm}(\theta', \phi'). \end{aligned}$$

In this case, we define a gauge potential

$$\Lambda_0^e(\mathbf{r}') = \sqrt{2\pi} \sum_{l=2}^{\infty} \frac{2l-1}{2l+1} \bar{f}_{l-1} \sum_{m=-l}^l \lambda_l^m \bar{X}_l^m(\mathbf{r}')$$

where $\bar{f}_l = R_0 \frac{X_l^1(\mathbf{r}_0)}{2l+1} \frac{N_l^1}{N_{l+1}^0} \sqrt{\frac{4\pi}{2l+1}}$; λ_l^m are unknown coefficients to be determined subsequently from the Coulomb gauge for the vector potential induced outside the sphere. Addition of $\nabla \Lambda_0^e$ to \mathbf{A}_0^e results in the replacement of the coefficients \mathbf{I}_l^m by

$$\begin{aligned} \mathcal{I}_l^m &= \mathbf{I}_l^m + \left(\frac{\mathbf{e}_\eta^*}{\sqrt{2}} N_{l+1}^{m-1} \lambda_{l+1}^{m-1} - \frac{\mathbf{e}_\eta}{\sqrt{2}} N_{l+1}^{m+1} \lambda_{l+1}^{m+1} \right. \\ &\quad \left. + \mathbf{e}_z N_{l+1}^m \lambda_{l+1}^m \right) / N_l^m. \end{aligned}$$

Now we can simply proceed to the frame of reference rotating together with the sphere by redefining the azimuthal angle as $\phi' = \phi'' + \Omega t$, where ϕ'' is the azimuthal angle in the rotating frame of reference and Ω is the dimensionless angular velocity of rotation. Respectively, the complex unit vector and the spherical harmonics change in a rotating frame of reference as $\mathbf{e}_\eta' = \mathbf{e}_\eta'' e^{i\Omega t}$ and $\bar{X}_l^m(\mathbf{r}') = \bar{X}_l^m(\mathbf{r}'') e^{im\Omega t}$. In a rotating frame of reference, the vector potential takes the form

$$\begin{aligned} \mathbf{A}_0^e(\mathbf{r}'') &= \sqrt{2\pi} \sum_{l=1}^{\infty} \bar{f}_l \sum_{m=-l}^l \left(\mathbf{e}_z'' (\mathbf{e}_z' \cdot \mathcal{I}_l^m) e^{im\Omega t} \right. \\ &\quad \left. + \mathbf{e}_\eta'' (\mathbf{e}_\eta'^* \cdot \mathcal{I}_l^m) e^{i(m+1)\Omega t} \right. \\ &\quad \left. + \mathbf{e}_\eta''^* (\mathbf{e}_\eta' \cdot \mathcal{I}_l^m) e^{i(m-1)\Omega t} \right) \bar{X}_l^m(\mathbf{r}''). \end{aligned}$$

Further we consider the current alternating harmonically with the dimensionless frequency $\bar{\omega}$ as $\mathbf{j}^e(\mathbf{r}', t) = \mathbf{j}_0^e(\mathbf{r}') \cos(\bar{\omega} t)$ and the vector potential alternating in the laboratory frame of reference, respectively, as

$$\mathbf{A}^e(\mathbf{r}', t) = \mathbf{A}_0^e(\mathbf{r}') \cos(\bar{\omega} t) = \Re [\mathbf{A}_0^e(\mathbf{r}') e^{i\bar{\omega} t}].$$

In the laboratory frame of reference, the complex amplitude of the vector potential induced outside the sphere is obtained as

$$\begin{aligned} \mathbf{A}_0^i(\mathbf{r}') &= \sqrt{2\pi} \sum_{l=1}^{\infty} \bar{f}_l \sum_{m=-l}^l \left(\mathbf{e}_\eta' (\mathbf{e}_\eta'^* \cdot \mathcal{I}_l^m) g_l^{m+1} \right. \\ &\quad \left. + \mathbf{e}_\eta'^* (\mathbf{e}_\eta' \cdot \mathcal{I}_l^m) g_l^{m-1} \right. \\ &\quad \left. + \mathbf{e}_z' (\mathbf{e}_z \cdot \mathcal{I}_l^m) g_l^m \right) X_l^m(\mathbf{r}') \end{aligned}$$

where $g_l^m = \frac{j_{l+1}(\sqrt{\bar{\omega}_m/i})}{j_{l-1}(\sqrt{\bar{\omega}_m/i})}$ and $\bar{\omega}_m = \bar{\omega} + m\bar{\Omega}$. From the Coulomb gauge $\nabla \cdot \mathbf{A}_0^i = 0$ we find

$$\begin{aligned} \lambda_{l+1}^m N_{l+1}^m &\left[\frac{1}{2(N_l^{m-1})^2} + \frac{1}{2(N_l^{m+1})^2} + \frac{1}{(N_l^m)^2} \right] = \\ &= \left[\frac{(\mathbf{e}_\eta'^* \cdot \mathcal{I}_l^{m-1})}{\sqrt{2}(N_l^{m-1})^2} - \frac{(\mathbf{e}_\eta' \cdot \mathcal{I}_l^{m+1})}{\sqrt{2}(N_l^{m+1})^2} - \frac{(\mathbf{e}_z' \cdot \mathcal{I}_l^m)}{(N_l^m)^2} \right] \end{aligned}$$

For the field induced outside the sphere we obtain

$$\begin{aligned} (\mathbf{r}' \cdot \nabla \times \mathbf{A}_0^i) &= i\pi \sum_{l=1}^{\infty} l \bar{f}_l \sum_{m=-l}^l g_l^m X_l^m(\mathbf{r}') \\ &\quad \times [N_{l+1}^{m-1} Y_{l+1}^{m-1}(\pi/2, 0) \\ &\quad + N_{l+1}^{m+1} Y_{l+1}^{m+1}(\pi/2, 0)]. \end{aligned}$$

The gauge potential Λ_0^e vanishes in the expression above and so it does not affect the total torque which is

$$\begin{aligned} \mathbf{M} &= \mathbf{e}_z' \frac{\pi}{2} \sum_{l=1}^{\infty} \frac{f_l^2}{(2l+1)^2(l+1)} \sum_{m=-l}^l \Im [g_l^m] \\ &\quad \times [(l-m+1)(l-m+2)\bar{P}_{l+1}^{m-1}(0)^2 \\ &\quad - (l+m+1)(l+m+2)\bar{P}_{l+1}^{m+1}(0)^2]. \end{aligned}$$

Other components of the torque, which are not parallel to the angular velocity of rotation, vanish because of $\bar{P}_l^m(0)\bar{P}_l^{m\pm 1}(0) = 0$. For slow rotations with $\bar{\Omega} \ll \bar{\omega}$ we have

$$g_l^m - g_l^{-m} = 2m\bar{\Omega}\partial_{\bar{\omega}} g_l + O(\bar{\Omega}^3)$$

that results in $\mathbf{M} \approx \mathbf{e}_z' \bar{\Omega} \partial_{\bar{\Omega}} \mathbf{M}$, where

$$\begin{aligned} \partial_{\bar{\Omega}} \mathbf{M} &= \pi \sum_{l=1}^{\infty} \frac{\Im [\partial_{\bar{\omega}} g_l] f_l^2}{(2l+1)^2(l+1)} \sum_{m=1}^l m \\ &\quad \times [(l-m+1)(l-m+2)\bar{P}_{l+1}^{m-1}(0)^2 \\ &\quad - (l+m+1)(l+m+2)\bar{P}_{l+1}^{m+1}(0)^2]. \end{aligned} \quad (13)$$

For the rest state of the sphere to be stable to rotational perturbations, the torque caused by these perturbations has to damp them that corresponds to $\partial_{\bar{\Omega}} \mathbf{M} < 0$. In the opposite case, the rest state is unstable. The state is marginally stable when $\partial_{\bar{\Omega}} \mathbf{M}(\bar{\omega}_c) = 0$, which is the equation defining the critical frequency $\bar{\omega}_c$ for the spin-up instability.

IV. NUMERICAL RESULTS

A. Small-amplitude oscillations

In the following we present some numerical results for an inductor consisting of two circular loops of equal radii placed coaxially at the distance H from the mid-plane. The current having the same amplitude may flow either in the same or in opposite directions in both loops. Subsequently, both these cases are referred to as symmetric and antisymmetric, respectively. We start with a simple symmetric case when both loops coincide ($H = 0$) making up a single loop with doubled current amplitude. The forces along with axial and radial spring constants versus the distance of the sphere from such a loop of dimensionless radius $R = 2$ are shown in Fig. 2 for various dimensionless frequencies. As seen in Fig. 2(a), at large enough distances the force, which is repulsive, raises with decreasing distance between the loop and the sphere. At some distance, the force attains a maximum and tends to zero as the sphere approaches the center of the loop. Such a reducing force implies that the position of the sphere is statically unstable to axial perturbations. The position is statically stable to axial perturbations when the axial spring constants shown in Fig. 2(b) are positive that requires the sphere to be placed further away from the loop than the point of maximum force which is at $z \approx 0.75$. A position being axially stable may become unstable radially when the distance from the loop becomes too large (see Fig. 2b). Thus the range of statically stable positions for a single loop is rather limited ($0.75 < z < 1.5$) and does not change significantly with the frequency of the magnetic field.

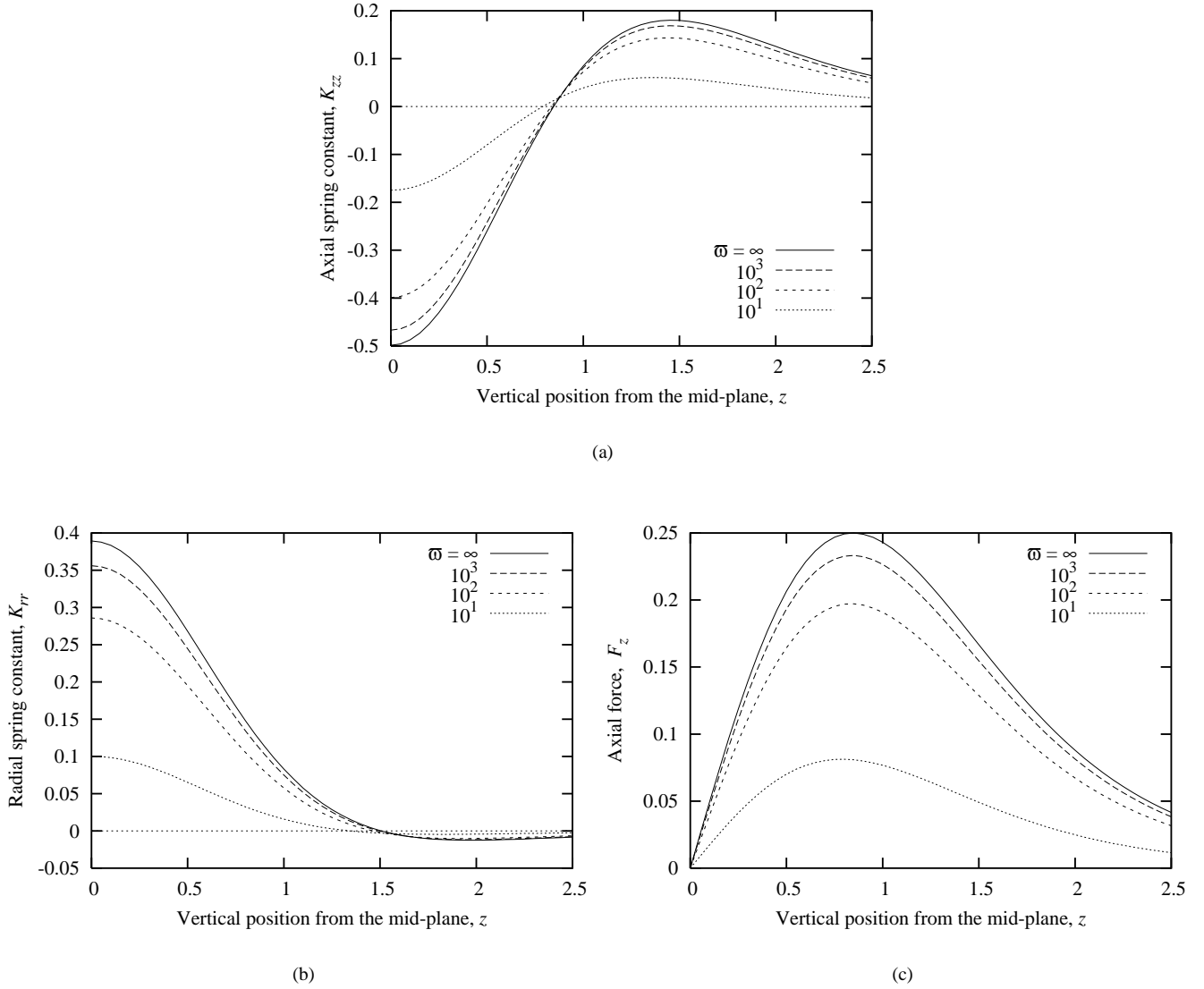


Fig. 2. Force (a), axial (b) and radial (c) spring constants in the magnetic field of a single loop with $R = 2$ versus the position of the sphere from the mid-plane at various dimensionless frequencies. A negative spring constant implies that the position is statically unstable.

Further let us turn briefly to the static stability of a sphere in an arrangement of two coaxial current loops of the same radius placed symmetrically at distance H from the center of the sphere. For the sake of brevity we restrict the static stability analysis to the perfect-conductor approximation $\bar{\omega} = \infty$. Axial and radial spring constants are shown in Fig. 3 versus the distance H at various radii of the loops for both symmetric and antisymmetric arrangements. In the symmetric arrangement, which is usually used for heating, the position of the sphere is statically unstable in radial direction when the loops are too much separated, and it becomes unstable in the axial direction when the loops are moved too tightly together. Overlapping of the stability ranges for radial and axial perturbations depends on the radius of the loops. For $R = 2$ the range of axial stability ends at $H \approx 1$ where the range of radial stability begins. Thus, there is no overlapping of the stability ranges in this case that implies a static instability regardless of the

distance between the loops. A range of positions statically stable to both axial and radial perturbations is possible only for sufficiently small radii of the loops. For instance at $R = 1.25$ this range is approximately $0.5 < z < 0.75$. In contrast to the symmetric arrangement, an antisymmetric one, which is usually used for positioning of the sample, ensures a statically stable state to radial perturbations regardless of the distance between the loops (see Fig. 3b on right). The position of the sphere is stable to axial perturbations for any radius of the loop provided the loops are separated by a distance larger than the radius of the sphere ($H > 0.5$). There might be an axial instability for smaller separations of the loops at $R < 2$ (see Fig. 3a on right).

Forces together with axial and radial spring constants versus the distance of the sphere from the mid-plane of both symmetric and antisymmetric arrangements of two loops are shown in Fig. 4 for various distances between the loops in the perfect-

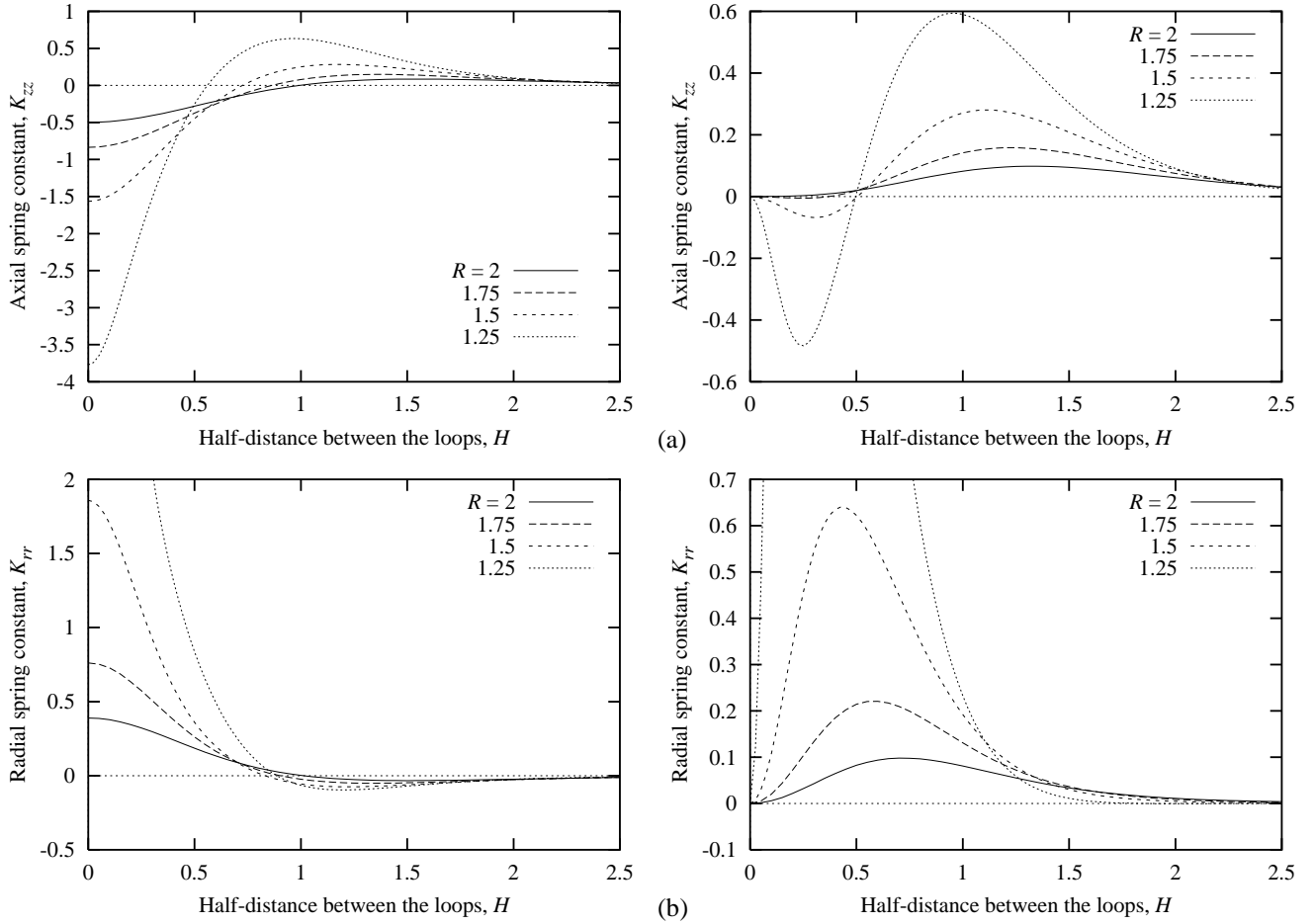


Fig. 3. Axial (a) and radial (b) spring constants versus the half-distance between the loops for both symmetric (on left) and antisymmetric (on right) arrangements at various radii of the loops in perfect-conductor approximation ($\bar{\omega} = \infty$).

conductor approximation ($\bar{\omega} = \infty$). It is seen that the position of the sphere in the middle-point ($z = 0$) of a symmetric arrangement (Fig. 4 on left) is unstable either in radial or axial directions for almost all distances between the coils. However, there is one distance between the coils, $H \approx 1$, at which both spring constants cross zero almost simultaneously. Thus, this distance is an optimal one for the static stability of the sphere in the middle-point. Note that the distance $H = R/2$ provides the most uniform magnetic field in the vicinity of the middle-point of the symmetric arrangement. This is because the next to the leading order contribution for the magnetic field of symmetric arrangement vanishes at the aspect ratio $H/R = \cot \theta_0 = 0.5$, i.e., $P_3^1(\cos \theta_0) = 0$ in (5). Similarly, the distance $H = R\sqrt{3}/2$ providing the most uniform gradient of the magnetic field in the vicinity of the middle-point of an antisymmetric arrangement is expected to ensure the widest range of statically stable positions for loops of large enough radius.

The dynamic stability of small-amplitude radial and axial oscillations is characterized by the corresponding growth rates Γ_{rr} and Γ_{zz} defined by (13). The threshold of linear stability is given by the frequency above which the corresponding growth rate becomes positive. At the threshold frequency, the amplitude of oscillations turns from decaying to growing in

time. A characteristic feature of this instability is that the growth rate, becoming positive above the threshold frequency, reaches a maximum at a certain frequency and tends to zero at higher frequencies. The frequency at which the growth rate attains a maximum is referred to as the most dangerous one. Threshold frequencies along with the most dangerous one and the corresponding maximal growth rates are plotted in Fig. 5 versus the half-distance between the loops at various radii of the loops for both axial and radial oscillations of a sphere about the middle-point of both symmetric and antisymmetric arrangements of two loops. The most dangerous frequency is always above the threshold one. As seen in Figs. 5(a) and 5(b), at large enough distances between the loops, the threshold and the most dangerous frequencies tend to $\bar{\omega}_c = 27.682$ and $\bar{\omega}_d = 47.196$ in the symmetric arrangement, and to $\bar{\omega}_c = 11.609$ and $\bar{\omega}_d = 18.792$ in the antisymmetric one, respectively. Note that these critical frequencies for the oscillatory instability in spatially quadratic and linear magnetic fields coincide with those for the spin-up instability in linear and uniform magnetic fields, respectively, which will be considered later. For each radius of a symmetric arrangement, there is a certain optimal distance between the loops that maximizes the critical frequency. For large enough radii the optimal distance between the loops is approximately equal to the radius, $2H = R$,

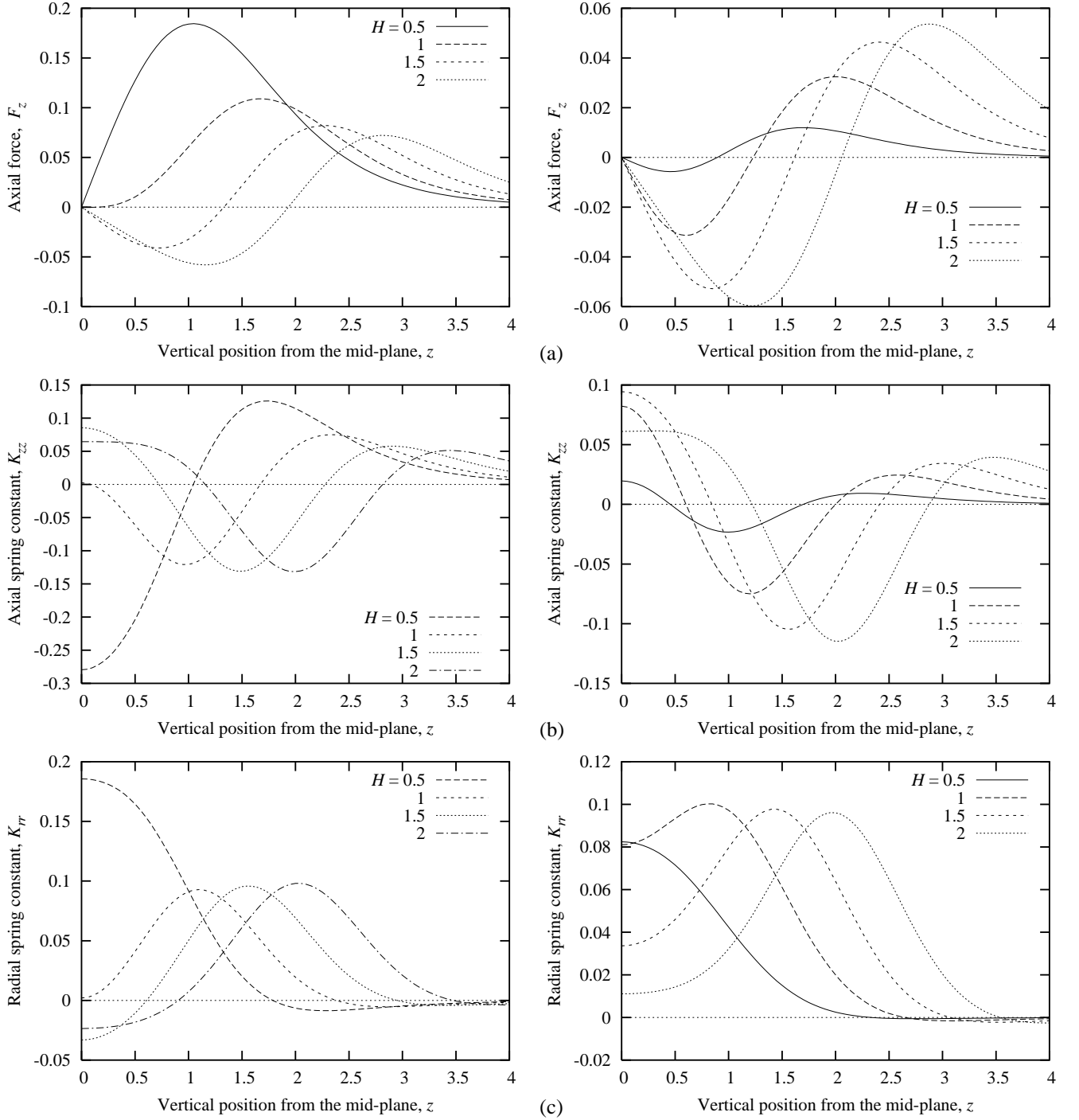


Fig. 4. Force (a), axial (b) and radial (c) spring constants versus the position of the sphere above the mid-plane for symmetric (on left) and antisymmetric (on right) arrangements of two coaxial loops of radius $R = 2$ and various distances from the mid-plane at $\bar{\omega} = \infty$.

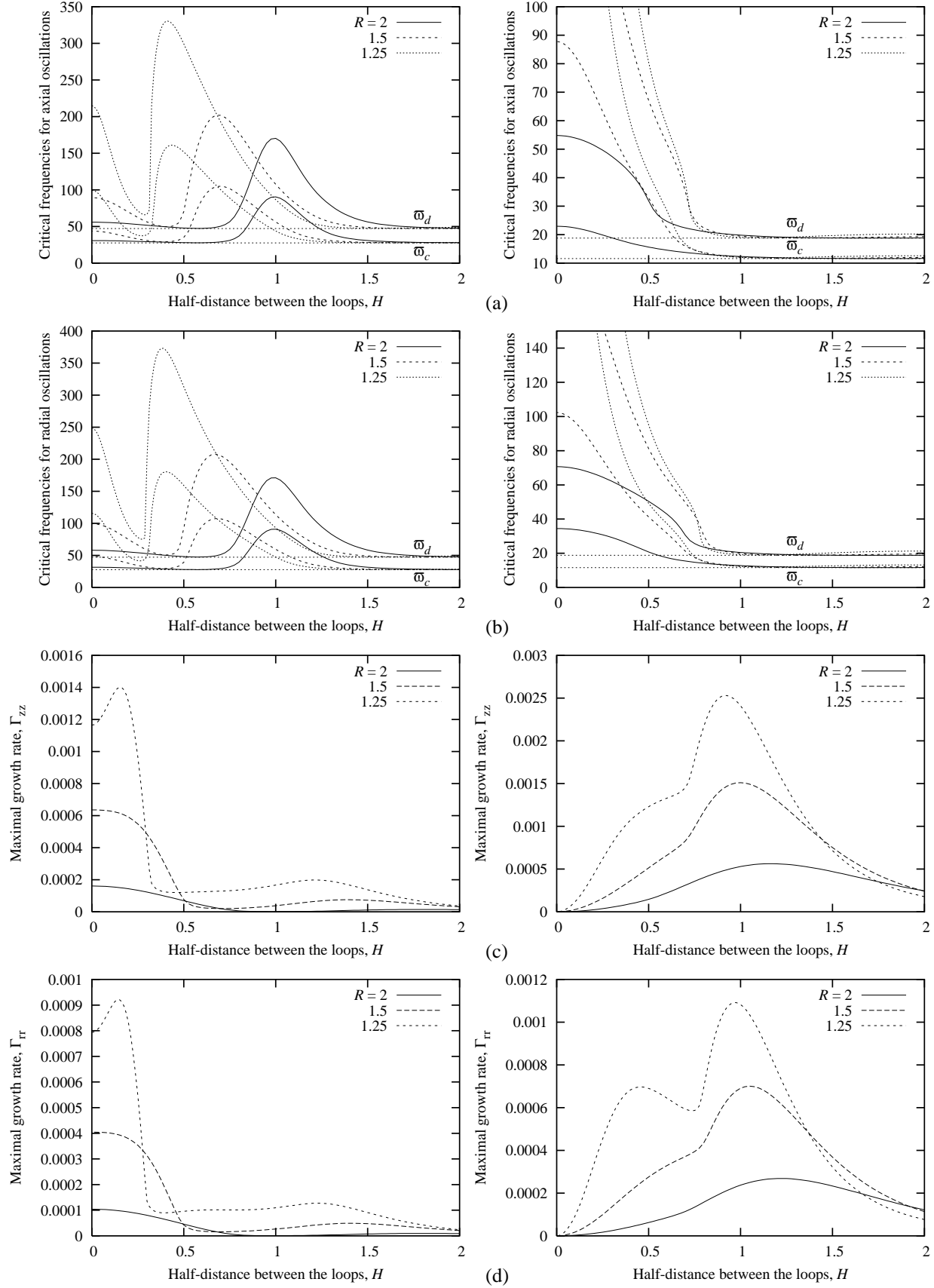


Fig. 5. Critical ($\bar{\omega}_c$) and most dangerous ($\bar{\omega}_d$) dimensionless AC frequencies (a, b) and maximal growth rates (c, d) for axial (a, c) and radial (b, d) oscillations of a sphere about the middle-point of symmetric (on left) and antisymmetric (on right) arrangements of two loops versus the half-distance between the loops at various radii of the loops.

which is optimal also for the static stability as considered above. With decreasing of the loop radius, the optimal distance becomes slightly larger (see Figs. 5a and 5b on left). In the antisymmetric case, the critical frequency changes weakly on reducing of the distance H until the loops approach a distance $H \approx 0.75$ to the mid-plane (see Figs. 5a and 5b on right). Further approaching of the loops results in the increase of the critical frequency which is the larger, the smaller the radius. This raise is caused by the nonuniformity of the magnetic field in the vicinity of the loop. Although the critical frequency for axial oscillations is, in general, slightly lower than that for the radial oscillations, there is no significant difference between both. The maximal growth rate for the symmetric case changes weakly with reducing distance between the loops until the distance becomes comparable to the radius of the sphere ($z \approx 0.5$) (see Figs. 5c and 5d on left). Closer approaching of the loops causes a significant increase of the growth rate for both axial and radial oscillations. Again, the smaller the radius of the loops, the larger the increase of the growth rate. In the antisymmetric case, the growth rate reaches a maximum as the loops approach to the mid-plane at a distance comparable to the radius of the sphere ($z \approx 1$) (see Figs. 5c and 5d on right).

B. Spin-up instability

Spin-up instability occurs when the frequency of the alternating magnetic field exceeds the threshold $\bar{\omega}_c$ defined above. The spin-up rate being proportional to $\partial_{\bar{\omega}} M$ becomes positive as the frequency raises over the threshold and attains a maximum at some higher frequency $\bar{\omega}_d$ subsequently referred to as the most dangerous one. These critical frequencies together with the corresponding maximal spin-up rates for a sphere at the middle-point between symmetric and antisymmetric arrangements of two loops are plotted in Fig. 6 versus the half-distance between the loops of various radii. As seen in Fig. 6(a), at large enough distances between the loops the threshold and the most dangerous frequencies tend to $\bar{\omega}_c = 11.609$ and $\bar{\omega}_d = 18.792$ in the symmetric arrangement, and to $\bar{\omega}_c = 27.682$ and $\bar{\omega}_d = 47.196$ in the antisymmetric one, which correspond to the spatially uniform and linear fields, respectively. In the symmetric case, the critical frequencies have a minimum at the distance between the loops equal to their radius: $2H = R$ (see Fig. 6a on left). Note that this is converse to the critical frequencies for the oscillatory instability considered previously which have a maximum at this distance. This minimum is due to the maximal uniformity of the field in the vicinity of the middle-point achieved at this distance between the loops. Critical frequencies increase with the non-uniformity of the field which becomes particularly significant when the loops are approached closer than the radius of the sphere ($H \approx 0.5$). In this case, the smaller the radius of the loops, the higher the critical frequencies. The spin-up rate raises as the loops are approached and attains a maximum at $H \approx 0.5$. For the loops with large enough radius the maximum of the spin-up rate is attained when both loops merge together forming a single one (see Fig. 6b on left). In the antisymmetric case, the critical frequencies begin to raise

significantly when the loops approach to the mid-plane at a distance of the radius of the sphere: $H \approx 1$ (see Fig. 6a on right). As seen in Fig. 6b on right, the spin-up rate attains a maximum approximately at the same distance.

V. SUMMARY AND CONCLUSIONS

This work presents an analytic stability analysis of a solid sphere levitated electromagnetically in an axisymmetric magnetic field induced by a set of coaxial circular loops. Stability is considered with respect to both oscillations of small amplitude and arbitrary direction and rotations perpendicular to the axis of symmetry of the field. Both oscillations and rotations are found to become growing in time when the dimensionless frequency of the field exceeds a certain critical threshold $\bar{\omega}_c$ depending on the configuration of the field for each kind of instability. The growth rates of both instabilities become positive as the frequency is raised over the corresponding threshold, attain a maximum at some higher frequency and tend to zero at high frequencies. The frequency $\bar{\omega}_d$, at which the maximum is attained, is referred to as the most dangerous one for the corresponding instability. Critical frequencies and the corresponding maximal growth rates are calculated for arrangements of two loops of the same radius carrying the same total current which may flow either in the same or in opposite directions. These arrangements, corresponding to the usual heating and positioning fields, are referred to as the symmetric and antisymmetric ones. It is found that critical frequencies for both oscillatory and rotational instabilities increase with the nonuniformity of the magnetic field. The lowest dimensionless critical frequencies are $\bar{\omega}_c = 11.609$ and $\bar{\omega}_d = 18.792$ which are the same for both the spin-up instability in a uniform magnetic field and the oscillatory instability in a spatially linear field. This coincidence represents a particular case of a more general rule: the critical frequencies for the spin-up instability in a spherically harmonic field of degree l coincide with the critical frequencies for oscillatory instability in a spherically harmonic field of degree $l + 1$. Thus, the critical frequencies $\bar{\omega}_c = 27.682$ and $\bar{\omega}_d = 47.196$ for the spin-up instability in a linear field coincide with the critical frequencies for the oscillatory instability in a spatially quadratic magnetic field which is the case at the mid-point of a symmetric arrangement of two loops except the case that the distance between the loops is equal to the radius of the loops. In this particular case, the quadratic term vanishes and the instability is dominated by the fourth-order term which has critical frequencies $\bar{\omega}_c = 85.252$ and $\bar{\omega}_d = 158.6$. Thus, the distance $2H = R$ is optimal in order to avoid the oscillatory instability of the sphere at the mid-point of the symmetric arrangement. This distance, which ensures the most uniform magnetic field at the middle-point, yields a minimum of the critical frequency for the spin-up instability. Note that there is no similar optimal distance for the oscillatory instability in antisymmetric arrangement where the critical frequency can be increased only by the nonuniformity of the magnetic field when the loops are approached close to the surface of the sphere. Hence, the stabilization of a sphere by an optimal design of the inductor is rather limited and active means of

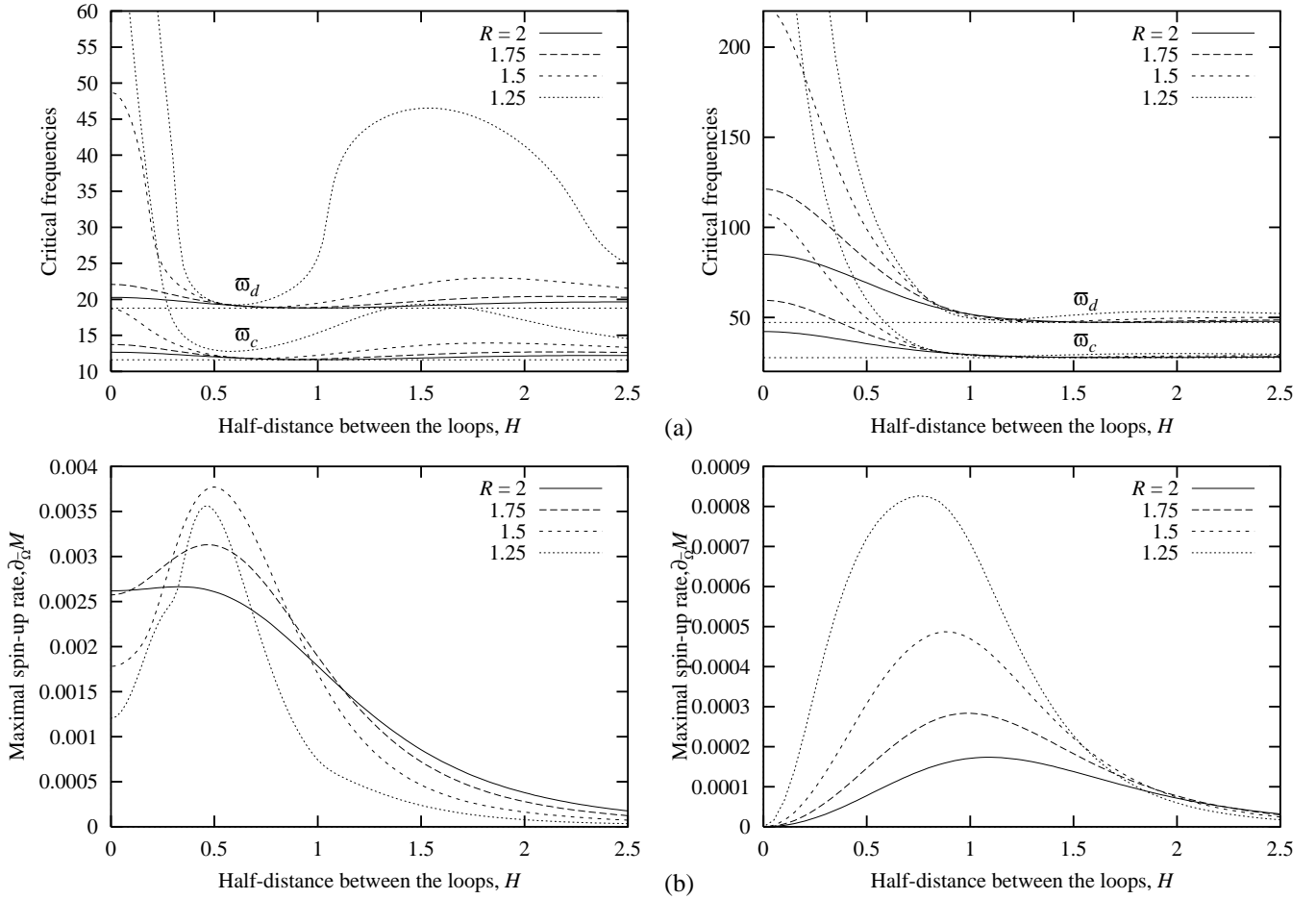


Fig. 6. Critical ($\bar{\omega}_c$) and most dangerous ($\bar{\omega}_d$) dimensionless AC frequencies (a) and maximal growth rates (b) for a spin-up instability in symmetric (on left) and antisymmetric (on right) arrangements of two loops versus the half-distance of the loops with various radii.

stabilization, like an additional steady magnetic field, may be necessary.

Note that the maximal dimensionless growth rates for both oscillatory and spin-up instabilities are small, typically $\Gamma \sim 10^{-3}$. From the physical point of view we have introduced the growth rate as a viscous-type friction coefficient at the velocity. Thus the physical dimension of Γ is s/m and, consequently, its scale is τ_m/R , because we have used the magnetic diffusion time τ_m and the radius of the sample R as time and length scales, respectively. In order to obtain the actual friction force we have to take the product of velocity, friction coefficient and the magnitude of the characteristic total electromagnetic force F_0 which usually is comparable to the gravity of the sample mg , where m is the mass of the sample and g the free fall acceleration. By comparing the negative effective friction force to the inertia we obtain an estimate of the characteristic growth time of the instability $\tau_0 \sim \frac{1}{\Gamma} \frac{R}{g\tau_m}$ which for a characteristic size $R \sim 10^{-2} m$ and a conductivity $\sigma \sim 10^6 \Omega^{-1}m^{-1}$ of the sample leads to $\tau_0 \sim 10^4 s$. Thus, although the magnetic field has a dynamically destabilizing effect, the development of the instability is expected to be very slow and, thus, hardly observable. In conclusion, note that the frequency of the magnetic field is the only parameter determining the threshold of dynamic instabilities as long as

no external damping, for instance due to a surrounding gas, is taken into account. In the opposite case, the threshold of instability would depend not only on the frequency but also on the amplitude of the current.

In conclusion note that the dynamic instabilities resulting from the effect of motion of a conducting body in an AC magnetic field can be interpreted from an alternative physical point of view which can explain the weakness of this instability and also suggests other possible instability mechanisms. In the given AC magnetic field, the electromagnetic force on the spherical body at rest depends only on its position. If the position changes, it takes some time for the electromagnetic force to relax to its time-averaged stationary value for the given position. This delay is caused by the finite time of magnetic diffusion in the body which, taking place over the skin depth, is thus comparable to the AC oscillation period τ . The electromagnetic force at instant t on the body in motion may be represented as $\mathbf{F}(\mathbf{r}(t - \tau))$. Assuming a sufficiently high AC frequency, we can expand this representation in a power series of small τ yielding $\mathbf{F}(\mathbf{r}(t - \tau)) \approx \mathbf{F}(\mathbf{r}(t) - \tau\mathbf{v}) \approx \mathbf{F}(\mathbf{r}(t)) - \tau(\mathbf{v} \cdot \nabla)\mathbf{F}$. Thus, the delay of the magnetic field results in a force component proportional to the velocity which is obviously analogous to a viscous friction force. Since for a statically stable position the effective electromagnetic

reaction force $(\mathbf{x} \cdot \nabla)\mathbf{F}$ is directed against the displacement \mathbf{x} , the effective friction force $-\tau(\mathbf{v} \cdot \nabla)\mathbf{F}$ is directed with the motion. Consequently, the delay of the magnetic field results in an effective electromagnetic friction force with a negative and, thus, destabilizing friction coefficient. It is important to note that the friction coefficient is small because it involves the delay time which is short and comparable to the AC period when the relaxation of the magnetic field is solely due to the electromagnetic diffusion over the skin depth. The same arguments may be extended to the coupling of the magnetic field and the temperature distribution in the body caused by its temperature-dependent electrical conductivity. In this case, the delay of the magnetic field would be dominated by the thermal relaxation time which is much longer than the electromagnetic diffusion time and, thus, expected to cause stronger dynamic instabilities than the pure electromagnetic mechanism considered here. In addition, the decrease of the electrical conductivity for increasing temperature, which is caused by the Joule heating of the AC magnetic field, and the related reduction of the non-dimensional frequency $\bar{\omega}$ might be important in levitation experiments.

APPENDIX I

APPROXIMATION OF A TOROIDAL INDUCTOR OF SMALL CROSS-SECTION BY A CIRCULAR LOOP

Consider a toroidal inductor of arbitrary cross-section carrying an axisymmetric and purely azimuthal current. The magnetic field of such an inductor may be represented as a superposition of the fields of separate circular loops constituting the inductor, and the corresponding vector potential may be written as the integral over the inductor cross-section S : $\mathbf{A}(\mathbf{r}) = \int_S \mathbf{A}_0(\mathbf{r}, \mathbf{r}') ds'$, where

$$\mathbf{A}_0(\mathbf{r}, \mathbf{r}') = \frac{1}{4\pi} \int_0^{2\pi} \frac{\mathbf{j} r' d\phi'}{|\mathbf{r} - \mathbf{r}'|}$$

is the nondimensionalized vector potential of a single circular loop defined by the radius vector $\mathbf{r}' = r' \mathbf{e}_r' + z' \mathbf{e}_z'$ with r' and z' being the radius and axial position of the loop in cylindrical coordinates. Subsequently assume the skin effect to be negligible as if the inductor would be fed by a direct current driven by the gradient of an electrostatic potential Φ . An axisymmetric and purely azimuthal current distribution with density $\mathbf{j} = j \mathbf{e}_\phi$ implies Φ to depend solely on the azimuthal angle ϕ . Consequently, $\mathbf{j} = -\nabla\Phi = \mathbf{e}_\phi \frac{1}{r} \frac{\partial\Phi}{\partial\phi}$, where $\frac{\partial\Phi}{\partial\phi} = C$ is a constant that can be related to the total current in the inductor $I_0 = \int_S j ds$ and its effective radius

$$\bar{R} = \frac{S}{\int_S \frac{ds}{r}} \quad (14)$$

as $C = I_0 \bar{R}/S$. Further we assume the inductor cross-section to be located about some position $\mathbf{r}_0 = r_0 \mathbf{e} + z_0 \mathbf{e}_z$, which will be specified later, and approximate the field distribution by the following multipole type expansion:

$$\begin{aligned} \mathbf{A}(\mathbf{r}) \approx & \frac{I_0 \bar{R}}{4\pi S} \int_0^{2\pi} \mathbf{e}'_\phi \\ & \times \int_S [1 + (\mathbf{r}' - \mathbf{r}_0) \cdot \nabla_0] \frac{ds' d\phi'}{|\mathbf{r} - \mathbf{r}_0|}, \end{aligned}$$

where the operator ∇_0 acts on \mathbf{r}_0 . Now, if we define \mathbf{r}_0 as the position of the mass center of the cross-section $\mathbf{r}_0 = \frac{1}{S} \int_S \mathbf{r} ds$, the second dipole-like term cancels in the expression above which, thus, reduces to

$$\mathbf{A}(\mathbf{r}) \approx \frac{\bar{I} r_0}{4\pi} \int_0^{2\pi} \frac{\mathbf{e}'_\phi d\phi'}{|\mathbf{r} - \mathbf{r}_0|}. \quad (15)$$

The last expression defines the vector potential of a circular loop located at \mathbf{r}_0 and carrying the effective current $\bar{I} = I_0 \bar{R}/r_0$. For example, in the case of an inductor represented by a torus with major and minor radii r_0 and r_1 , the effective radius can easily be found from (14) as $\bar{R} = \frac{r_0}{2} \left(1 + \sqrt{1 + \left(\frac{r_1}{r_0} \right)^2} \right)$ while the mass center of the cross-section coincides with its geometrical center. Note that the solution (15) is accurate up to the quadrupole-like term neglected in (15) the magnitude of which relative to the remaining term may be estimated as $\sim |\mathbf{r}' - \mathbf{r}_0|^2 / |\mathbf{r} - \mathbf{r}_0|^2 \sim (d/R)^2$, where d is the characteristic size of the cross-section and R is the characteristic distance to the cross-section center. Obviously, the neglected term becomes significant only at distances comparable to d .

APPENDIX II

PROPERTIES OF THE FUNCTIONS $X_l^m(\mathbf{r})$ AND $\bar{X}_l^m(\mathbf{r})$.

Similarly to Ref. [11] we also use a complex unity vector $\mathbf{e}_\eta = \frac{1}{\sqrt{2}} (\mathbf{e}_x + i \mathbf{e}_y)$, where \mathbf{e}_x and \mathbf{e}_y are the corresponding Cartesian unit vectors, and employ the outer and inner solutions of the scalar Laplace equation, $X_l^m(\mathbf{r}) = r^{-l-1} Y_{l,m}(\theta, \phi)$ and $\bar{X}_l^m(\mathbf{r}) = r^l Y_{l,m}(\theta, \phi)$ associated with the spherical harmonic $Y_{l,m}(\theta, \phi)$ [13]. These variables provide a simple algebra for calculation of the gradient operator $\nabla = \mathbf{e}_\eta \frac{\partial}{\partial \eta^*} + \mathbf{e}_\eta^* \frac{\partial}{\partial \eta} + \mathbf{e}_z \frac{\partial}{\partial z}$ used throughout this study:

$$\begin{aligned} \frac{\partial X_l^m}{\partial \eta} &= \frac{1}{\sqrt{2}} \frac{N_{l+1}^{m-1}}{N_l^m} X_{l+1}^{m+1}, \\ \frac{\partial X_l^m}{\partial z} &= -\frac{N_{l+1}^m}{N_l^m} X_{l+1}^m, \\ \frac{\partial \bar{X}_l^m}{\partial \eta} &= \frac{1}{\sqrt{2}} \frac{2l+1}{2l-1} \frac{N_l^m}{N_{l-1}^{m+1}} \bar{X}_{l-1}^{m+1}, \\ \frac{\partial \bar{X}_l^m}{\partial z} &= \frac{2l+1}{2l-1} \frac{N_l^m}{N_{l-1}^m} \bar{X}_{l-1}^m, \end{aligned}$$

where the asterisk denotes the complex conjugate and $N_l^m = \sqrt{\frac{(l-m)!(l+m)!}{2l+1}}$. The corresponding relations for the complex conjugate functions follow straightforwardly from the above relations and the property of spherical harmonics: $Y_{l,m}^*(\theta, \phi) = (-1)^m Y_{l,-m}(\theta, \phi)$. Another relation used for the calculation of the torque in Sec. 3 is:

$$\begin{aligned} \mathbf{r} \times \nabla X_l^m &= i \left[\frac{\mathbf{e}_\eta^*}{\sqrt{2}} \frac{N_{l+1}^{m+1}}{N_l^m} (l-m) X_{l+1}^{m+1} \right. \\ &\quad + \frac{\mathbf{e}_\eta}{\sqrt{2}} \frac{N_{l+1}^{m-1}}{N_l^m} (l+m) X_{l+1}^{m-1} \\ &\quad \left. + \mathbf{e}_z m X_l^m \right]. \end{aligned}$$

Note that our definition of X_l^m is slightly different from that used in [11] leading to a bit more complicated algebra but simpler resulting expressions.

APPENDIX III

CALCULATION OF THE COEFFICIENTS $g_l(z)$.

The coefficients $g_l(z)$ and $g'_l(z)$ in (10,13, 13) can efficiently be calculated using continued fractions [16]. For this purpose we rewrite $g_l(z) = \frac{j_{l+1}(z)}{j_{l-1}(z)} = h_l(z)h_{l-1}(z)$ where $h_l(z) = \frac{j_{l+1}(z)}{j_l(z)}$ and $j_l(z)$ is the spherical Bessel function of index l . Further, applying a recurrence relation for the spherical Bessel function of index $l+1$ we obtain the continued fraction:

$$h_l(z) = \frac{1}{(2l+3)/z - h_{l+1}(z)} \\ = \frac{1}{(2l+3)/z - \frac{1}{(2l+5)/z - \frac{1}{(2l+7)/z - \dots}}}$$

allowing us to calculate $h_l(z)$ provided that $h_{l+1}(z)$ is known. But asymptotic properties of Bessel functions suggest that for large index l $h_l(z) \sim \frac{z}{2l}$. Thus for any z we can choose sufficiently large l' and then truncate the fraction by approximating $h_{l'}(z)$ by the previous expression that allows us to calculate back the necessary $h_l(z)$. Note that the forward recurrence for $h_l(z)$ is not practically applicable because it is numerically unstable similarly to its counterpart for Bessel functions. The other necessary quantity $g'_l(z) = \frac{dg_l}{dz}$, contained in (13,13), can be calculated in a similar way by expressing it as $g'_l(z) = (2l+1)(h_{l-1}^2(z) - g_l(z))/z$. For $\bar{\omega} \gg 1$ we have $g_l(\sqrt{\bar{\omega}/i}) \sim -1 + \frac{2l+1}{\sqrt{i\bar{\omega}}}$ which follows from the corresponding asymptotics of the Bessel functions [13].

REFERENCES

- [1] O. Muck, German patent 422004, Oct. 30, 1923.
- [2] E. C. Okress, D. M. Wroughton, G. Comenetz, P. H. Brace, J. C. R. Kelly, "Electromagnetic levitation of solid and molten metals," *J. Appl. Phys.*, vol. 23, pp. 545–552, 1952.
- [3] I. Egry, A. Diefenbach, W. Dreier and J. Piller, "Containerless processing in space - thermophysical property measurements using electromagnetic levitation," *Int. J. Thermophys.*, vol. 22 no. 2, pp. 569–578, 2001.
- [4] I. Egry, G. Lohoefer, and G. Jacobs, "Surface tension of liquid metals: results from measurements on ground and in space," *Phys. Rev. Lett.*, vol. 75, pp. 4043–4046, 1995.
- [5] G. Lohoefer, J. Brillo, I. Egry, "Thermophysical properties of under-cooled Liquid Cu-Ni alloys," *Int. J. Thermophys.*, vol. 25, pp. 1535–1550, 2004.
- [6] J. R. Hull and D. M. Rote, "Magnetohydrodynamic stability in the electromagnetic levitation of horizontal molten-metal sheets," *Phys. Fluids A*, vol. 1(6), pp. 1069–1076, 1989.
- [7] B. Abedian and R. W. Hayers, "Spin-up acceleration of levitated molten drop in MHD-flow instability," In *Proc. Int. Conf. on EPM*, pp. 267–272, Lyon, Oct. 14–17, 2003.
- [8] H. Keissig and U. Essman, "Preparation of metals in ultra high vacuum by electromagnetic levitation," *Mater. Res. Bull.*, vol. 14, pp. 1139–1145, 1979.
- [9] J. Priede and G. Gerbeth, "Spin-up instability of electromagnetically levitated spherical bodies," *IEEE Trans. Magn.*, vol. 36, pp. 349–353, 2000.
- [10] J. Priede and G. Gerbeth, "Oscillatory instability of electromagnetically levitated solid bodies," *IEEE Trans. Magn.*, vol. 36, pp. 354–357, 2000.
- [11] G. Lohoefer, "Force and torque of an electromagnetically levitated metal sphere," *Q. Appl. Math.*, vol. 51, pp. 495–518, 1993.
- [12] G. Lohoefer, "An electrically conducting sphere in a three-dimensional, alternating magnetic field," *IMA J. Appl. Math.*, vol. 68, pp. 1–21, 2003.
- [13] M. Abramowitz and I. A. Stegun, *Handbook of mathematical functions*. New York: Dover, 1965.
- [14] J. D. Jackson, *Classical electrodynamics*. Second edition. New York: Wiley, 1975.
- [15] W. R. Smythe, *Static and dynamic electricity*, McGraw-Hill, New York: 1950.
- [16] W. H. Press *et al.*, *Numerical recipes in Fortran*, New York: Cambridge, 1992.